N88-27160

COMPARISON OF EXPERIMENTAL COUPLED HELICOPTER ROTOR/BODY STABILITY RESULTS WITH A SIMPLE ANALYTICAL MODEL*

P. P. Friedmann+ and C. Venkatesan++
Mechanics and Structures Department
University of California
Los Angeles, CA 90024

Summary

This paper presents the results of an analytical study aimed at predicting the aeromechanical stability of a helicopter in ground resonance, with the inclusion of aerodynamic forces. The theoretical results are found to be in good agreement with the experimental results, available in the literature, indicating that the coupled rotor/fuselage system can be represented by a resonably simple mathematical model.

Nomenclature

a	= lift curve slope
$C(k)$	= Theodorsen's lift deficiency function
c_{d0}	= profile drag coefficient of the blade
e	= hinge offset
f	= rotating natural frequency
h_2	= height of rotor hub above the gimbal
$I_{xx}, I_{xy}, I_{yy}, I_{yx}$	= rotary inertia of the model about the gimbal axes
K_β, K_ζ	= stiffness of the root springs of the blade in flap and lag respectively
m	= mass/unit length of the blade
R	= rotor radius
s	= complex eigenvalue
t	= time
β_{nc}, β_{ns}	= n - cosine, n-sine flap coordinates
β_p	= blade precone, in the equations
β_p	= progressing flap mode (high frequency) in the figures only
β_R	= regressing flap mode (low frequency)
β_o	= rotor blade equilibrium angle in flap
β_{1c}, β_{1s}	= cyclic flap coordinates
$\Delta\beta_k$	= time dependent perturbations of the k^{th} blade in flap
ϵ	= order of magnitude used for ordering various quantities
ζ_P	= progressing lag mode (high frequency)
ζ_R	= regressing lag mode (low frequency)
ζ_{1c}, ζ_{1s}	= cyclic lag coordinates
ζ_o	= rotor blade equilibrium angle in lag
$\Delta\zeta_k$	= time dependent perturbations of the k^{th} blade in lag
ζ_{nc}, ζ_{ns}	= n - cosine, n - sine lag coordinates
θ	= body pitch
θ_c	= collective pitch setting of the blade
θ_{eff}, θ_o	= effective angle of attack
θ_{ZL}	= zero lift angle of attack
λ	= inflow ratio
σ	= model damping (real part of s)
$\bar{\sigma}$	= solidity ratio
ϕ	= body roll
ψ	= nondimensional time (Ωt)
ω	= modal frequency (imaginary part of s)
Ω	= rotor R.P.M.

Presented at the Integrated Technology Rotor (ITR) Methodology Assessment Workshop, NASA Ames Research Center, Moffett Field, CA., June 21-22, 1983.

*This work was supported by NASA Ames Research Center under Grant NAG 2-116.

+Professor of Engineering and Applied Science

++Assistant Research Engineer

$(\bar{\ })$ = nondimensionalized quantity, with respect to R when involving length, and with respect to Ω when involving frequency

$(')$ = $\frac{d}{d\psi}$

I. Introduction

The aeromechanical instability of a helicopter, on the ground and in flight, is caused by coupling between the rotor and the body degrees of freedom. This instability is commonly denoted air resonance when the helicopter is in flight and ground resonance when the helicopter is on the ground. The physical phenomenon involved during this instability is quite complex, the rotor lead-lag regressing mode usually couples with the body pitch or roll to cause the instability. The nature of the coupling which is both aerodynamic and inertial is introduced in the rotor due to body or support motion. Development of a mathematically consistent model capable of representing the coupled rotor/fuselage dynamic system is of fundamental importance for the study of these type of problems. The mathematical model should be consistent because the geometrically nonlinear terms associated with moderate blade deflections are known to have a significant role in rotary wing aeroelasticity[1]. Thus various terms having the same order of magnitude must be retained throughout the derivation of the equations of motion. A consistent mathematical model has been developed[2,3], by the authors, to study the aeroelastic, structural dynamic and aeromechanical effects in multi-rotor systems.

Bousman[4] has obtained excellent experimental data for aeromechanical stability of a hingeless rotor on a special gimbaled support simulating body pitch and roll degrees of freedom. The availability of this high quality experimental data provides an opportunity for comparing the results obtained from the analytical model with this experimental data. Bousman attributed some of the discrepancies found between the theoretical results presented in his paper and experimental results to dynamic inflow. This conclusion was also examined by Johnson[5], in a recent study, where unsteady aerodynamic effects on the rotor was represented by a perturbation inflow model[6]. Johnson showed that theoretical results based on his model[7], with dynamic inflow provided results which showed better agreement with the experimental results than the results based on a quasi-steady aerodynamic model without dynamic inflow. He concluded from his study that unsteady aerodynamic effects are represented quite well by a dynamic inflow model.

Using the mathematical model developed by the authors[2,3], it is shown that the theoretical results, based on the quasi-steady aerodynamic model, are for most cases in better agreement with the experimental results than the agreement noted by Bousman[4]. The agreement with the experimental data is also comparable to that obtained by Johnson[5], except that the quasi steady model is incapable of predicting the "dynamic inflow mode" found by Johnson[5], which is a result of the augmented state due to inflow dynamics.

The good agreement between the analytical and experimental results indicates that the relatively simple analytical model is accurate for this case. Furthermore it also implies that only part of the discrepancy between theory and experiment, found by Bousman, may be attributed to dynamic inflow.

II. A Brief Summary of the Experiment

A clear description of the experimental set up, used for simulating the fundamental aspects of the aeromechanical stability of a hingeless rotor helicopter, is presented in Ref. 4. The rotor consisted of three blades and five different configurations were tested. The different configurations represent different blade parameters characterized by the nonrotating natural frequencies of the blade in flap and lag, pitch-lag coupling and flap-lag coupling. The rotor was designed such that most of the blade flexibility is concentrated at the root by building in root flexures. The rotor assembly was supported on a gimbal which had pitch and roll degrees of freedom. In this paper the analytical results obtained were compared with the experimental results, presented by Bousman, for rotor configurations 1 and 4, where the designation of these configurations is consistent with those in Bousman's paper[4].

A brief description of these configurations is presented for the sake of completeness. Configuration 1 had different stiffnesses in flap and lag respectively, the corresponding nonrotating flap frequency was 3.13 Hz and that for lead-lag was 6.70 Hz. Configuration 4 was a matched stiffness case where the nonrotating flap frequency was 6.63 Hz and that for lead-lag was 6.73 Hz. The airfoil cross-section of the blade was cambered and had a zero lift angle of attack equal to -1.5 degrees. Thus a substantial part of the experimental data was obtained for zero pitch setting, however, due to the presence of camber the rotor produces a small amount of thrust at this pitch setting. The rotor blades were rigid outboard of the flap and lag flexures which were located at a radial station 0.105R. There was no flap-pitch or pitch-lag couplings for these two configurations (configurations 1 and 4). Furthermore, the blade was very stiff in torsion. In the case of the experiments conducted for pitch angles other than zero, the experimental set up was so designed as to introduce the changes in pitch angle outboard of the flexures and hence there was no flap-lag structural coupling for these cases. The structural damping in body roll was very small in comparison with that for body pitch. The body pitch and roll frequencies were controlled by cantilever springs on which the gimbal was mounted. It is stated in Ref. 4 that the body pitch spring was selected to provide a dimensionless body pitch frequency of about 0.12 at the nominal rotor speed of 720 R.P.M. and the roll spring was selected to give a dimensionless

roll frequency of about 0.28. (The frequencies are nondimensionalized by dividing by rotor speed.) Based on these values, the dimensional frequencies in pitch and roll are 1.44 Hz and 3.36 Hz respectively. It was also mentioned in Ref. 4 that the dimensional values of the body pitch and roll frequencies are about 2 Hz and 4 Hz respectively. So the difference, noted between the two sets of body frequencies, raises a question as to what are the exact values for the pitch and roll frequencies. However the experimental results presented in Ref. 4 showed that over a wide range of Ω (200 ~ 1000 R.P.M.) the pitch and roll frequencies are very close to 2 Hz and 4 Hz respectively. Hence, for the present analysis, the pitch and roll frequencies are selected to be 2 Hz and 4 Hz. The reason for choosing 2 Hz and 4 Hz for body frequencies was that at approximately 750 R.P.M., the lead-lag regressing mode of the rotor was close to the body roll frequency causing an aeromechanical instability. The data used in our calculations, is presented in the Appendix B.

III. Description of the Analytical Model

The analytical model used to study this aeromechanical stability problem is based on the equations developed for a multi-rotor system presented in Ref. 2 and 3. Those equations represent the dynamics of the coupled rotor/vehicle system consisting of two rotors interconnected by a flexible structure. The various degrees of freedom considered, in deriving the equations, are flap, lag, torsion for each blade, rigid body translation and rotation of the complete vehicle and also the degrees of freedom representing the normal modes of vibration of the supporting structure. From this multi-rotor analytical model, only those degrees of freedom and the corresponding equations of motion that are relevant for the present study have been retained. The most important assumptions upon which the formulation is based on are: (1) the rotor consists of 3 or more number of blades, (2) the rotor is lightly loaded, (3) the rotor is in uniform inflow, and (4) the rotor blade is modelled as a rigid blade with orthogonal springs located at the root of the blade (Fig. 1), where K_β and K_ζ represent the stiffness of the blade in flap and lag motions.

The aerodynamic model is based on Greenberg's[8] derivation of unsteady aerodynamic loads on an oscillating airfoil in a pulsating flow. This theory is basically a modified form of Theodorsen's unsteady aerodynamic theory. By assuming the Theodorsen's lift deficiency function $C(k) = 1$ and neglecting the torsional motion of the blade, the aerodynamic model becomes a simple quasi-steady model with apparent mass terms. In the present calculations, only this quasi-steady aerodynamic model with apparent mass terms is used. It was found from our calculations that neglecting the apparent mass terms from the aerodynamic model affects the results only by 2 ~ 4%.

The inflow ratio λ, used in the calculation of the aerodynamic loads was evaluated from[6]

$$\lambda = \frac{\bar{\sigma}a}{16}\left[\sqrt{1 + \frac{24\,\theta_{eff}}{\bar{\sigma}a}} - 1\right] \qquad (1)$$

where $\bar{\sigma}$ is the solidity ratio

a is the lift curve slope

and θ_{eff} is the effective angle of attack of the blade.

As indicated in Ref. 4, a cambered airfoil was used in the model rotor tested, thus

$$\theta_{eff} = \theta_c - \theta_{ZL} \qquad (2)$$

where θ_c is the collective pitch setting of the blade

θ_{ZL} is the zero lift angle of attack.

The zero lift angle of attack, for the airfoil employed[4] (NACA 23012), was $\theta_{ZL} = -1.5$ degrees.

As mentioned earlier, the equations of motion are nonlinear, because geometrical nonlinearities due to moderate deflection of the blade are included. Retention of the nonlinear terms is based upon an ordering scheme[1,2]. The blade degrees of freedom, representing blade slopes are assigned an order of magnitude represented by a symbolic quantity ε, and are denoted to be of order $0(\varepsilon)$, where $0.1 < \varepsilon < 0.15$. The fuselage degrees of freedom are assumed to be of a slightly smaller magnitude $0(\varepsilon^{3/2})$. As indicated in Ref. 1, this assumption is quite important for obtaining equations which are manageable from an algebraic point of view. The ordering scheme consists of neglecting terms of order $0(\varepsilon^2)$ when compared to order one, thus $1 + 0(\varepsilon^2) \simeq 1$.

The degrees of freedom considered in this aeromechanical stability analysis are: the fundamental flap and lag modes for each blade and the pitch and roll degrees of freedom of the body. In this class of problems, it has been established that the collective flap and lag modes do not couple with the body motion and thus, these modes are not considered. Therefore, the total number of degrees of freedom governing the aeromechanical problem are six. These consist of: cyclic flap (β_{1c},β_{1s}), cyclic lead-lag (ζ_{1c},ζ_{1s}), body pitch (θ) and body roll (ϕ).

IV. Method of Solution and Discussion of Results

The method of solution for coupled rotor/fuselage problem follows essentially the procedure explained in Ref. 1 and 3. A brief outline of the procedure is given in the following few paragraphs.

The equations of motion, for coupled rotor/fuselage problem, are usually nonlinear

differential equations with periodic coefficients. These differential equations can be either ordinary or partial depending on the type of model used for the representation of the rotor blade. If the blade is modelled as a rigid blade with root springs, the resulting equations will be nonlinear ordinary differential equations. On the other hand, if the blade is modelled as a flexible beam, the final equations will be nonlinear partial differential equations. In this case, the partial differential equations are first transformed into ordinary differential equations using Galerkin's method. Thereafter the method of solution is the same regardless which of these two blade models is used. In the present case, because the blade is modelled as rigid blade with root springs (Fig. 1), the equations of motion are nonlinear ordinary differential equations with periodic coefficents. The steps involved, in solving these equations to obtain the stability information, are as follows.

1. Evaluation of the equilibrium position for the blade.

2. Linearization of the nonlinear ordinary differential equations about the equilibrium position. (Linearized equations will have periodic coefficients.)

3. Transformation of the linearized equations with periodic coefficients to linearized equations with constant coefficients, by applying multiblade coordinate transformation.

4. Evaluation of the eigenvalues of the linearized system with constant coefficients to obtain the information about the stability.

For the case of hover, the equations which represent the static equilibrium of the blade are obtained by imposing the requirement that all time derivatives of the blade degrees of freedom and the fuselage perturbations vanish in the equations. The resulting equations are nonlinear algebraic equations and they are identical for all the blades in the rotor indicating that the static equilibrium is same for all blades. This static equilibrium position is obtained by solving the nonlinear algebraic equations using a numberical method, namely the Newton-Raphson technique. Then the blade degrees of freedom are expressed as time varying perturbations about the static equilibrium position, β_0 and ζ_0 for flap and lag respectively.

$$\beta_k(\psi) = \beta_0 + \Delta\beta_k(\psi)$$

$$\zeta_k(\psi) = \zeta_0 + \Delta\zeta_k(\psi)$$

Substituting these into the nonlinear ordinary differential equations of motion and neglecting terms which contain the product of the perturbation terms, yields the linearized equations of motion. The linearized equations for the k-th blade will have periodic coefficients, since the k-th blade equations are written in the blade fixed rotating coordinate system. Transformation of the perturbations equations to a nonrotating system will result in equations with constant coefficients. This transformation is performed using the multiblade coordinate transformation[6]. During this transformation, the individual blade degrees of freedom will transform to a new se of rotor degrees of freedom. In the past, these rotor degrees of freedom have been referred to as multiblade coordinates or Coleman coordinates or Fourier coordinates or rotor-plane coordinates. These coordinates are basically representative of the behavior of the rotor as a whole when viewed from a nonrotating frame. For the sake of completeness the equations of blade equilibrium, the linearized perturbational blade equations (in the multiblade or rotor plane coordinate system) and the perturbational equations for the pitch and roll degrees of freedom are presented in Appendix A.

Stability of the linearized system is determined by performing an eigen-analysis on the linearized constant coefficient perturbation equations. The eigen-values appear as complex pairs $s = \sigma \pm i\omega$. The complex part of the eigen value (ω) refers the modal frequency and the real part (σ) refers the modal damping. The mode is stable if σ is negative and it is unstable if σ is positive.

For the present problem, there are six pairs of complex eigen-values each one representing one of the six degrees of freedom, namely, β_{1c}, β_{1s}, ζ_{1c}, ζ_{1s}, θ and ϕ. The modes corresponding to the rotor degrees of freedom (β_{1c}, β_{1s}, ζ_{1c}, ζ_{1s}) are referred to either progressing mode or regressing mode. The designation of progressing or regressing to a particular mode is based on the numerical value of the rotating natural frequency of the rotor. Suppose the rotating natural frequency, say in lead-lag, is f/rev. Then the two frequencies corresponding to the cyclic lag modes (ζ_{1c}, ζ_{1s}) will be (f+1)/rev and (f-1)/rev, where f+1 is the high frequency lag mode and f-1 is the low frequency lag mode. If f is greater than 1/rev, the high frequency lag mode (f+1) is a progressing mode and the low frequency lag mode (f-1) is a regressing mode. On the other hand, if f is less than 1/rev, the high frequency lag mode is a progressing mode and the low frequency lag mode is also a progressing mode. These designations are also applicable for the flap modes of the rotor. A clear description of these is given in Ref. 6. For a stiff-in-plane rotor, the rotating natural frequency in lead-lag greater than 1/rev. Hence the high frequency lead-lag mode is a progressing mode and the low frequency lead-lag mode is a regressing mode. For a soft inplane rotor since the rotating natural frequency is less than 1/rev, both high frequency and low frequency lag modes are progressing modes.

In the present study, aimed at the aeromechanical stability of a model helicopter, the behavior of the model is studied at various Ω's of the rotor. Thus due to the variation in Ω, a stiff inplane rotor at low Ω's will become a soft inplane rotor at high Ω's. In the experiment performed by Bousman[4], the flexibility of the blade in lead-lag is such that the rotor becomes a soft inplane rotor beyond Ω = 445 R.P.M. Hence, for Ω < 445 R.P.M., the lead-lag modes will have one progressing mode and one regressing mode and for Ω > 445 R.P.M., both the lag modes will be progressing modes. In Refs. 4 and 5, even for Ω > 445 R.P.M., the low-frequency lag mode is referred as regressing mode instead of progressing mode. The reason could be to avoid any confusion while referring to various modes. So, for the sake of consistency, during the discussion of our results, the low frequency lag mode is always referred as lag regressing mode.

The results for configuration 1 are presented in Figs. 2-7, while the results for configuration 4 are presented in Figs. 8-12. The variation of the various modal frequencies with Ω are presented in Fig. 2, together with the experimental data obtained in Ref. 4. The progressing flap and progressing lead-lag frequencies increase very rapidly with Ω. The lead-lag regressing mode frequency evaluated from the analytical model is in excellent agreement with the experimental results. The body pitch and roll frequencies have slightly higher values than the experimental results. The damping in pitch as a function Ω is shown in Fig. 3. The analytical results are in relatively good agreement with the experimental data. The variation of the damping in roll as a function of Ω is shown in Fig. 4. It is evident that for this case the analytical results yield values which are somewhat higher than the experimental data. The differences observed between our analytical results and the experimental points, for the frequency and damping in body modes, could be explained as follows. In our calculations, the numerical values used for the stiffness and structural damping in body pitch and roll modes are evaluated based on pitch frequency equal to 2 Hz and roll frequency equal to 4 Hz. As pointed out in Sec. II of this paper, there is some doubt about the correctness of the body frequencies (2 and 4 Hz) because in Ref. 4, there are two different sets of frequencies for pitch and roll, namely 1.44 and 3.36 Hz, and 2 and 4 Hz respectively.

Figure 5 represents the variation of damping in lead-lag regressing mode with Ω. As indicated before, Johnson's results[5] show that the theory with inflow dynamics shows better agreement with experimental data than the theory with quasi-steady aerodynamics. However, even with quasi-steady aerodynamics, the results of the present analysis show slightly better agreement than the results obtained in Ref. 5 with inflow dynamics. It is also important to note that in the region, beyond 800 R.P.M., our results are in excellent agreement with the experimental data, while the theory with inflow dynamics predicts higher values.

Results from the calculations performed indicated that the progressing and regressing flap modes are always stable and the damping in these modes increases monotonically with Ω for configuration 1 as well as for configuration 4. Since these modes are always stable, the results are not presented in this paper.

Changes in the damping of the lead-lag regressing mode as a function of the collective pitch setting of the blade are presented in Fig. 6. Since Johnson[5] has not presented a corresponding set of results, it was not possible to compare these results with an analysis based on the dynamic inflow model. At Ω = 650 R.P.M., the results shown in Fig. 6a indicate that the theoretical analysis used by Bousman[4] predicts a much lower value for the damping than the experimental results. The present analysis shows considerably better agreement. It should be noted however that for larger values of pitch setting the difference between the predicted results and the experimental results increases. This difference could be attributed to the simple quasi-steady aerodynamic model used in our analysis. This difference however is much smaller than the one exhibited by Bousman's results. Even more interesting are the results presented in Fig. 6b, corresponding to Ω=900 R.P.M. For this case experimental results indicate a lead-lag regressing mode which is always stable, but the theoretical results shown by Bousman[4] imply an instability which becomes stronger beyond a collective pitch setting of 2 degrees. As evident from Fig. 6b, the results of our analysis predict the correct trend and the predicted damping levels are much closer to the experimental results. It should be noted again that the agreement between the predicted and experimental results diminishes with increasing collective pitch setting. An item to be noted in these figures (6a, 6b) is that the curve representing our analytical results starts from an angle θ_c = -1.5 degrees. Although Fig. 6 contains an experimental data point corresponding to θ_c = -3 degrees, we have not computed the results for this pitch setting because for θ_c = -3 degrees, the relation between inflow ratio and the collective pitch of the blade (Eq. 1) becomes indeterminate.

The variations in pitch damping as a function of collective pitch setting are shown in Fig. 7a, and similar variations for roll damping are shown in Fig. 7b. As evident from 7b, the damping in roll is predicted quite well. However the damping in pitch predicted by the present analysis is much lower than the experimental results. One can only speculate on the possible cause for this discrepancy. One possible reason could be the slight nonlinearity present in the structural damping in pitch mentioned in Ref. 4.

At Ω = 650 R.P.M., the lead-lag regressing mode frequency is close to the body pitch frequency (Fig. 2) and therefore the amplitudes in pitch could be higher. Thus nonlinearity in structural damping in pitch could manifest itself by increasing the total damping in pitch.

The results for configuration 4 are presented next. The variation of modal frequencies with Ω are shown in Fig. 8. The lead-lag regressing mode frequency is in excellent agreement with our analytical predictions. The pitch and roll frequencies are predicted well. Bousman's[4] experiments showed the presence of a frequency of about 0.8 Hz beyond Ω = 350 R.P.M., whereas the present analysis has not predicted any frequency close to this value. Note that the regressing flap mode frequency is close to the pitch mode over a wide range of $\Omega(400 < \Omega < 1000$ R.P.M.). Thus it is possible that the pitch mode can be excited by the proximity of the regressing flap mode. The explanation for the presence of the 0.8Hz frequency, measured in the test, posed a problem since the theoretical results presented by Bousman[4] as well as those obtained by Johnson[5], with the quasi-steady aerodynamics, were incapable of predicting a 0.8Hz frequency. It is quite relevant to quote Bousman on this matter, Ref. 4, p. 53. In Bousman's words, "However in the experimental case, measurements in the pitch coordinate show two modes of comparable damping at rotor speeds beyond 350 R.P.M., one mode at about 0.8 Hz and the other at 2.0 Hz". Bousman refers one as pitch mode (0.8 Hz) and the other as flap regressing mode (2.0 Hz). However, in identifying these modes Bousman states, "To call one mode the body mode, and the other flap regressing mode is somewhat arbitrary; the rationale used here is that as the blade pitch angle increases only one of these modes remains, and it is assumed to be the body pitch mode". But Johnson[5], using the inflow dynamics model, was able to predict theoretically a frequency close to 0.8 Hz and he called it as the inflow mode and he identified the other frequency (2.0 Hz) as the pitch mode. Quoting Johnson, Ref. 5, p. 672, "That it is measurable (i.e., 0.8 Hz inflow mode) is surprising, since in fact the inflow variables λ_x and λ_y do not correspond to real physical states of the system". He proceeds to interpret this behavior as "the unsteady aerodynamics introduces behavior of the system, as observed in either time or frequency domain, that can be approximated by an additional oscillatory mode with low or moderate damping. Approximating the behavior by an additional mode implies then the existence of additional states or degrees of freedom of the system". Johnson also states that this behavior is observed only for matched stiffness case because "the flap regressing mode will be more coupled with the body motion". But examination of Fig. 6 in Ref. 5 (the results based on the theory with inflow dynamics) reveals that the flap regressing mode frequency is not near the body pitch frequency, so it is questionable whether coupling could occur between these two modes. In our analysis, however the results show that the flap regressing mode is close to the body pitch mode, as indicated in Fig. 8. Thus it appears that the interpretation offered by Johnson for the presence of the 0.8 Hz frequency mode and its designation as the inflow mode frequency is possible, albeit speculative.

The variation of lead-lag regressing mode damping with Ω is presented in Fig. 9. Again, the present analytical results are in closer agreement with the experimental results than those predicted by the theory with inflow dynamics. Figure 10 and 11 show the variation of damping in roll and pitch modes with Ω. The pitch damping is predicted well. The roll damping is overestimated.

The variation in damping levels of the lead-lag regressing mode with collective pitch angle, of the blade are shown in Fig. 12, for two different values of angular speed. It is evident from Fig. 12b that for the case of Ω=1000 R.P.M., the theory used by Bousman predicts an unstable region beyond θ_c = 3 degrees, however the experiment indicates a stable configuration. The results of the present analysis are in good agreement with the experimental results. The agreement noted in Figs. 6 and 12, between the analytical results of our study and the experimental data, for nonzero values of collective pitch, seems to indicate that the discrepancy between theory and experiment for these cases, evident in Ref. 4, could be associated with the details of the mathematical model and is not related to unsteady aerodynamic effects such as dynamic inflow.

V. Concluding Remarks

In this paper, the results of a theoretical analysis, of the aeromechanical stability of a hingeless rotor helicopter, are compared with the experimental results. Using a quasi-steady aerodynamic model, it was found that the results of the present analysis compare quite well with the experimental results. It is interesting to note that this correlation with experimental data appears to hold in both the region of zero collective pitch angles considered by Johnson[5] as well as in the nonzero range of collective pitch angles which was considered by Bousman[4], but not by Johnson. Obviously the quasi steady aerodynamic model is incapable of predicting the "dynamic inflow mode" which is caused by the augmented state of the system, when the dynamic inflow model is used. In an extension of this study which will include dynamic inflow, the physical meaning of the dynamic inflow mode will be reexamined.

This study also indicates that the discrepancy between the predicted values of regressing mode lag damping and the experimental measurements, noted in Ref. 4, for configurations 1 and 4, do not seem to be associated with dynamic inflow and are more likely to be related to the details of the mathematical model.

Furthermore the analytical model used in this study has the capability of simulating the experiment, with good accuracy, because it is based on the same blade model which was actually tested.

Finally, it should be noted that the analytical model was based on an ordering scheme where blade slopes were assumed to be of order ϵ and the fuselage rotations in pitch and roll were assumed to be of order $\epsilon^{3/2}$, which leads to simplification in the equations of motion. The cases considered in the present study (both experimental and theoretical) were restricted so that only the linear first order terms in fuselage rotations were important. Thus other classes of problems, in which nonlinear terms in fuselage rotations are also exercised, have to be considered to determine the overall reliability of this particular ordering scheme.

Acknowledgment

The authors would like to express their gratitude to W. Bousman, W. Johnson and H. Miura for the constructive comments they have made on the draft version of this paper.

References

1. Friedmann, P.P., "Formulation and Solution of Rotary-Wing Aeroelastic Stability and Response Problems", Presented at the Eighth European Rotorcraft Forum at Aix-En-Provence, France, Aug. 31-Sep. 3, 1982, Published in Vertica, Vol. 7, No. 2, 1983, pp. 101-141.

2. Venkatesan, C. and Friedmann, P.P., "Aeroelastic Effects in Multirotor Vehicles with Application to Hybrid Heavy Lift System, Part I: Formulation of Equations of Motion", Submitted to NASA for publication as a Contractor Report, Dec. 1982.

3. Venkatesan, C. and Friedmann, P.P., "Aeroelastic Effects in Multirotor Vehicles, Part II: Method of Solution and Results Illustrating Coupled Rotor/Body Aeromechanical Stability", NASA CR Report in preparation.

4. Bousman, W.G., "An Experimental Investigation of the Effects of Aeroelastic Couplings on Aeromechanical Stability of a Hingeless Rotor Helicopter", Journal of the American Helicopter Society, Vol. 26, No. 1, Jan. 1981, pp. 46-54.

5. Johnson, W., "Influence of Unsteady Aerodynamics on Hingeless Rotor Ground Resonance, Journal of Aircraft, Vol. 19, No. 8, Aug. 1982, pp. 668-673.

6. Johnson, W., Helicopter Theory, Princeton University Press, Princeton, New Jersey, 1980.

7. Johnson, W., "A Comprehensive Analytical Model of Rotorcraft Aerodynamics and Dynamics", NASA TM 81182, June 1980.

8. Greenberg, J.M., "Airfoil in Sinusoidal Motion in a Pulsating Flow, NACA TN 1326, 1947.

Appendix A: Equations Used in this Study

The equations of blade equilibrium, the linearized perturbational blade equation in multiblade coordinates, together with the perturbational equations in the pitch and roll degrees of freedom are given below.

Equilibrium Equations

Flap:

$$\begin{aligned}
&\beta_0\{\bar{\omega}_F^2 + (\bar{\omega}_L^2 - \bar{\omega}_F^2)\sin^2\theta_c + \frac{\bar{\ell}^3}{3} + \frac{\bar{\ell}^2}{2}\bar{e}\} \\
&+ \zeta_0\{(\bar{\omega}_L^2 - \bar{\omega}_F^2)\sin\theta_c\cos\theta_c + \nu\frac{\bar{\ell}^4}{4}\beta_p\} \\
&+ \beta_0\zeta_0\{\nu\frac{\bar{\ell}^4}{4}\} \\
&+ \beta_p\{\frac{\bar{\ell}^3}{3} + \frac{\bar{\ell}^2}{2}\bar{e}\} - \nu\{\frac{\bar{\ell}^4}{4}\theta_0 + \\
&+ \frac{\bar{\ell}^3}{3}(-\lambda + 2\bar{e}\theta_0) - \frac{\bar{\ell}^2}{2}\bar{e}\lambda\} = 0
\end{aligned} \tag{A.1}$$

Lead-Lag

$$\begin{aligned}
&\beta_0\{-(\bar{\omega}_L^2 - \bar{\omega}_F^2)\sin\theta_c\cos\theta_c\} \\
&+ \zeta_0\{-\bar{\omega}_L^2 + (\bar{\omega}_L^2 - \bar{\omega}_F^2)\sin^2\theta_c - \frac{\bar{\ell}^2}{2}\bar{e} + \\
&+ \nu(-\frac{\bar{\ell}^4}{4}\beta_p\theta_0 - \frac{\bar{\ell}^3}{3}2\lambda\beta_p)\} + \beta_0\zeta_0\{\nu\frac{\bar{\ell}^3}{3}\lambda\} \\
&+ \nu\{-\frac{c_{d0}}{a}(\frac{\bar{\ell}^4}{4} + 2\frac{\bar{\ell}^3}{3}\bar{e}) - \frac{\bar{\ell}^3}{3}\lambda\theta_0 + \\
&+ \frac{\bar{\ell}^2}{2}\lambda(\lambda - \bar{e}\theta_0)\} = 0
\end{aligned} \tag{A.2}$$

where

$$\bar{\omega}_F^2 = \frac{K_\beta}{m\Omega^2R^3}$$

$$\bar{\omega}_L^2 = \frac{K_\zeta}{m\Omega^2R^3}$$

$$\nu = \frac{\rho_A abR}{m}\ ;\ \bar{e} = \frac{e}{R}\ ;\ \bar{\ell} = 1 - \bar{e}$$

When there is no structural flap-lag coupling, the terms containing $\sin\theta_c$ and $\cos\theta_c$ must be deleted from the above equations as well as in the stability equations given below.

$$\theta_0 = \theta_c - \theta_{ZL}$$

where θ_0 is the effective angle of attack

θ_c is the collective pitch setting of the blade

θ_{ZL} is the zero lift angle of attack

Linearized Stability Equations

n-cosine Flap

$$\beta_{nc}F_{nc}(1) + \beta_{ns}F_{nc}(2) + \zeta_{nc}F_{nc}(3) + \zeta_{ns}F_{nc}(4) + \dot{\beta}_{nc}F_{nc}(5) + \dot{\beta}_{ns}F_{nc}(6) + \dot{\zeta}_{nc}F_{nc}(7) + \ddot{\beta}_{nc}F_{nc}(8) + \ddot{\theta}F_{nc}(9) + \dot{\theta}F_{nc}(10) + \dot{\phi}F_{nc}(11) = 0 \qquad (A.3)$$

where

$$F_{nc}(1) = \bar{\omega}_F^2 + (\bar{\omega}_L^2 - \bar{\omega}_F^2)\sin^2\theta_c + \nu\frac{\bar{\ell}^4}{4}\zeta_0 + \frac{\bar{\ell}^3}{3} + \frac{\bar{\ell}^2}{2}\bar{e} - n^2\frac{\bar{\ell}^3}{3} - n^2\frac{1}{2}\nu\bar{b}\frac{\bar{\ell}^3}{3}\cos\theta_0$$

$$F_{nc}(2) = n(\nu\frac{\bar{\ell}^4}{4} + \nu\frac{\bar{\ell}^3}{3}\bar{e} + \bar{g}_{SF})$$

$$F_{nc}(3) = (\bar{\omega}_L^2 - \bar{\omega}_F^2)\sin\theta_c\cos\theta_c + \nu\frac{\bar{\ell}^4}{4}(\beta_p + \beta_0)$$

$$F_{nc}(4) = (2\frac{\bar{\ell}^3}{3}(\beta_0 + \beta_p) - 2\nu\frac{\bar{\ell}^4}{4}\theta_0 + \nu\frac{\bar{\ell}^3}{3}\lambda)n$$

$$F_{nc}(5) = \nu\frac{\bar{\ell}^4}{4} + \nu\frac{\bar{\ell}^3}{3}\bar{e} + \bar{g}_{SF}$$

$$F_{nc}(6) = n\{2\frac{\bar{\ell}^3}{3} + 2\frac{1}{2}\nu\frac{\bar{\ell}^3}{3}\bar{b}\cos\theta_0\}$$

$$F_{nc}(7) = 2\frac{\bar{\ell}^3}{3}(\beta_0 + \beta_p) - 2\nu\frac{\bar{\ell}^4}{4}\theta_0 + \nu\frac{\bar{\ell}^3}{3}\lambda$$

$$F_{nc}(8) = \frac{\bar{\ell}^3}{3} + \frac{1}{2}\nu\bar{b}\frac{\bar{\ell}^3}{3}\cos\theta_0$$

$$F_{nc}(9) = -\frac{\bar{\ell}^3}{3}\delta_n$$

$$F_{nc}(10) = -\delta_n\nu\frac{\bar{\ell}^4}{4}$$

$$F_{nc}(11) = \delta_n\{2\frac{\bar{\ell}^3}{3} + \bar{h}_2(2\nu\frac{\bar{\ell}^3}{3}\theta_0 - \nu\frac{\bar{\ell}^2}{2}\lambda)\}$$

where $\delta_n = 1$ when $n = 1$

$= 0$ $n \neq 1$

$\bar{g}_{SF} = \dfrac{g_{SF}}{m\Omega R^3}$; g_{SF} = damping in flap

b = semichord

n-Sine Flap

$$\beta_{ns}F_{ns}(1) + \beta_{nc}F_{ns}(2) + \zeta_{ns}F_{ns}(3) + \zeta_{nc}F_{ns}(4) + \dot{\beta}_{ns}F_{ns}(5) + \dot{\beta}_{nc}F_{ns}(6) + \dot{\zeta}_{ns}F_{ns}(7) + \ddot{\beta}_{ns}F_{ns}(8) + \ddot{\phi}F_{ns}(9) + \dot{\phi}F_{ns}(10) + \dot{\theta}F_{ns}(11) = 0 \qquad (A.4)$$

where

$$F_{ns}(1) = \bar{\omega}_F^2 + (\bar{\omega}_L^2 - \bar{\omega}_F^2)\sin^2\theta_c + \nu\frac{\bar{\ell}^4}{4}\zeta_0 + \frac{\bar{\ell}^3}{3} + \frac{\bar{\ell}^2}{2}\bar{e} - n^2\frac{\bar{\ell}^3}{3} - \frac{1}{2}\nu\bar{b}\frac{\bar{\ell}^3}{3}n^2\cos\theta_0$$

$$F_{ns}(2) = n\{-\nu\frac{\bar{\ell}^4}{4} - \nu\frac{\bar{\ell}^3}{3}\bar{e} - \bar{g}_{SF}\}$$

$$F_{ns}(3) = (\bar{\omega}_L^2 - \bar{\omega}_F^2)\sin\theta_c\cos\theta_c + \nu\frac{\bar{\ell}^4}{4}(\beta_0 + \beta_p)$$

$$F_{ns}(4) = n\{-2\frac{\bar{\ell}^3}{3}(\beta_0 + \beta_p) + 2\nu\frac{\bar{\ell}^4}{4}\theta_0 - \nu\frac{\bar{\ell}^3}{3}\lambda\}$$

$$F_{ns}(5) = \nu\frac{\bar{\ell}^4}{4} + \nu\frac{\bar{\ell}^3}{3}\bar{e} + \bar{g}_{SF}$$

$$F_{ns}(6) = n\{-2\frac{\bar{\ell}^3}{3} - 2\frac{1}{2}\nu\frac{\bar{\ell}^3}{3}\bar{b}\cos\theta_0\}$$

$$F_{ns}(7) = 2\frac{\bar{\ell}^3}{3}(\beta_0 + \beta_p) - 2\nu\frac{\bar{\ell}^4}{4}\theta_0 + \nu\frac{\bar{\ell}^3}{3}\lambda$$

$$F_{ns}(8) = \frac{\bar{\ell}^3}{3} + \frac{1}{2}\nu\bar{b}\frac{\bar{\ell}^3}{3}\cos\theta_0$$

$$F_{ns}(9) = \delta_n\frac{\bar{\ell}^3}{3}$$

$$F_{ns}(10) = \delta_n\nu\frac{\bar{\ell}^4}{4}$$

$$F_{ns}(11) = \delta_n\{2\frac{\bar{\ell}^3}{3} + 2\nu\frac{\bar{\ell}^3}{3}\theta_0\bar{h}_2 - \bar{h}_2\nu\frac{\bar{\ell}^2}{2}\lambda\}$$

n - Cosine lead-lag

$$\zeta_{nc}L_{nc}(1) + \zeta_{ns}L_{nc}(2) + \beta_{nc}L_{nc}(3) + \beta_{ns}L_{nc}(4) + \dot{\zeta}_{nc}L_{nc}(5) + \dot{\zeta}_{ns}L_{nc}(6) + \dot{\beta}_{nc}L_{nc}(7) + \dot{\beta}_{ns}L_{nc}(8) + \ddot{\zeta}_{nc}L_{nc}(9) + \ddot{\beta}_{nc}L_{nc}(10) + \ddot{\phi}L_{nc}(11) + \ddot{\theta}L_{nc}(12) + \dot{\theta}L_{nc}(13) = 0 \qquad (A.5)$$

where

$$L_{nc}(1) = -\bar{\omega}_L^2 + (\bar{\omega}_L^2 - \bar{\omega}_F^2)\sin^2\theta_c - \frac{\bar{\ell}^2}{2}\bar{e} + n^2\frac{\bar{\ell}^3}{3} - \nu\frac{\bar{\ell}^4}{4}\beta_p\theta_0$$

$$L_{nc}(2) = -n\{2\nu\frac{c_{d0}}{a}\frac{\bar{\ell}^4}{4} + \nu\frac{\bar{\ell}^3}{3}\theta_0\lambda + \bar{g}_{SL}\}$$

$$L_{nc}(3) = -(\bar{\omega}_L^2 - \bar{\omega}_F^2)\sin\theta_c\cos\theta_c - n^2\frac{1}{2}\nu\bar{b}\frac{\bar{\ell}^3}{3}\sin\theta_0$$

$$L_{nc}(4) = n\{2\frac{\bar{\ell}^3}{3}(\beta_0 + \beta_p) - \nu\frac{\bar{\ell}^4}{4}\theta_0 - \nu\frac{\bar{\ell}^3}{3}(-2\lambda + \bar{e}\,\theta_0)\}$$

$$L_{nc}(5) = -2\nu \frac{c_{d0}}{a} \frac{\bar{\ell}^4}{4} - \nu \frac{\bar{\ell}^3}{3} \theta_0\lambda - \bar{g}_{SL}$$

$$L_{nc}(6) = -n\, 2 \frac{\bar{\ell}^3}{3}$$

$$L_{nc}(7) = 2 \frac{\bar{\ell}^3}{3} (\beta_0+\beta_p) - \nu \frac{\bar{\ell}^4}{4} \theta_0 - \nu \frac{\bar{\ell}^3}{3} (-2\lambda + \bar{e}\theta_0)$$

$$L_{nc}(8) = 2n \frac{1}{2} \nu \bar{b} \frac{\bar{\ell}^3}{3} \sin\theta_0$$

$$L_{nc}(9) = - \frac{\bar{\ell}^3}{3}$$

$$L_{nc}(10) = \frac{1}{2} \nu \bar{b} \frac{\bar{\ell}^3}{3} \sin\theta_0$$

$$L_{nc}(11) = \delta_n \{ \frac{\bar{\ell}^3}{3} (\beta_p+\beta_0) + \bar{h}_2 \frac{\bar{\ell}^2}{2} \}$$

$$L_{nc}(12) = \delta_n \bar{h}_2 \frac{\bar{\ell}^2}{2} \zeta_0$$

$$L_{nc}(13) = \delta_n \{\nu \frac{\bar{\ell}^4}{4} \theta_0 - \frac{\bar{\ell}^3}{3} 2\lambda\nu\}$$

where $\bar{g}_{SL} = g_{SL}/m\Omega R^3$; g_{SL} = damping in lag

n-Sine lead-lag

$$\zeta_{ns}L_{ns}(1) + \zeta_{nc}L_{ns}(2) + \beta_{ns}L_{ns}(3) + \beta_{nc}L_{ns}(4) + \dot{\zeta}_{ns}L_{ns}(5) + \dot{\zeta}_{nc}L_{ns}(6) + \dot{\beta}_{ns}L_{ns}(7) + \dot{\beta}_{nc}L_{ns}(8) + \ddot{\zeta}_{ns}L_{ns}(9) + \ddot{\beta}_{ns}L_{ns}(10) + \ddot{\theta}\, L_{ns}(11) + \dot{\phi}\, L_{ns}(12) + \dot{\phi}\, L_{ns}(13) = 0 \qquad (A.6)$$

where

$$L_{ns}(1) = -\bar{\omega}_L^2 + (\bar{\omega}_L^2 - \bar{\omega}_F^2)\sin^2\theta_c - \frac{\bar{\ell}^2}{2} \bar{e} + n^2 \frac{\bar{\ell}^3}{3} - \nu \frac{\bar{\ell}^4}{4} \beta_p\theta_o$$

$$L_{ns}(2) = n\{2\nu \frac{c_{d0}}{a} \frac{\bar{\ell}^4}{4} + \nu \frac{\bar{\ell}^3}{3} \lambda\, \theta_0 + \bar{g}_{SL}\}$$

$$L_{ns}(3) = -(\bar{\omega}_L^2 - \bar{\omega}_F^2)\sin\theta_c\cos\theta_c - n^2 \frac{1}{2} \nu\bar{b} \frac{\bar{\ell}^3}{3} \sin\theta_0$$

$$L_{ns}(4) = n\{-2 \frac{\bar{\ell}^3}{3} (\beta_0+ \beta_p)+ \nu \frac{\bar{\ell}^4}{4} \theta_0 + \nu \frac{\bar{\ell}^3}{3} (-2\lambda + \bar{e}\theta_0) \}$$

$$L_{ns}(5) = -2\nu \frac{c_{d0}}{a} \frac{\bar{\ell}^4}{4} -\nu \frac{\bar{\ell}^3}{3} \lambda\, \theta_0 - \bar{g}_{SL}$$

$$L_{ns}(6) = 2n \frac{\bar{\ell}^3}{3}$$

$$L_{ns}(7) = 2 \frac{\bar{\ell}^3}{3} (\beta_p+\beta_0) -\nu \frac{\bar{\ell}^4}{4} \theta_0 -\nu \frac{\bar{\ell}^3}{3} (-2\lambda + \bar{e}\theta_0)$$

$$L_{ns}(8) = -2n \frac{1}{2} \nu \bar{b} \frac{\bar{\ell}^3}{3} \sin\theta_0$$

$$L_{ns}(9) = - \frac{\bar{\ell}^3}{3}$$

$$L_{ns}(10) = \frac{1}{2} \nu \bar{b} \frac{\bar{\ell}^3}{3} \sin\theta_0$$

$$L_{ns}(11) = \delta_n \frac{\bar{\ell}^3}{3} (\beta_p+ \beta_0) + \frac{\bar{\ell}^2}{2} \bar{h}_2\}$$

$$L_{ns}(12) = -\delta_n \bar{h}_2 \frac{\bar{\ell}^2}{2} \zeta_0$$

$$L_{ns}(13) = \delta_n\{-\nu \frac{\bar{\ell}^4}{4} \theta_0 + \frac{\bar{\ell}^3}{3} 2\lambda\nu\}$$

Roll

$$\frac{N}{2} m\Omega^2R^3\{\beta_{1c}<\nu \frac{c_{d0}}{a} \frac{\bar{\ell}^4}{4} + \nu \frac{\bar{\ell}^3}{3} \lambda\theta_0 + \bar{g}_{SF} + \nu \frac{\bar{\ell}^4}{4} + 2\nu \frac{\bar{\ell}^3}{3} \bar{e} + \bar{h}_2(\nu \frac{\bar{\ell}^3}{3} (\beta_p+\beta_0) + \nu \frac{\bar{\ell}^3}{3} \theta_o\zeta_o + \frac{1}{2} \nu \bar{b} \frac{\bar{\ell}^2}{2} \sin\theta_0) >$$

$$+ \beta_{1s} < -2\nu \frac{\bar{\ell}^4}{4} \zeta_0 + \nu\frac{\bar{\ell}^4}{4} (\beta_p+ 3\beta_0)\theta_0 + \frac{1}{2} \nu \bar{b} \frac{\bar{\ell}^3}{3} \cos\theta_0 + \bar{h}_2 (2\nu \frac{\bar{\ell}^3}{3} \theta_0 - \frac{\bar{\ell}^2}{2} \beta_p - \bar{\ell}^2 \beta_0 + \nu \frac{\bar{\ell}^2}{2} (-3\lambda + \bar{e}\theta_0)) >+ \zeta_{1c} < -\nu \frac{\bar{\ell}^4}{4} \theta_0 + \bar{h}_2\nu \frac{\bar{\ell}^3}{3} \theta_0(-\beta_p+ \beta_0) >+ \zeta_{1s} < \nu \frac{\bar{\ell}^4}{4} \zeta_0 2\theta_0 - \nu \frac{\bar{\ell}^4}{4} (\beta_p+ \beta_0)+ \beta_p\bar{g}_{SL} - \bar{h}_2 (\bar{\ell}^2\zeta_0 - 2\nu \frac{c_{d0}}{a} \frac{\bar{\ell}^3}{3} - \nu \frac{\bar{\ell}^2}{2} \lambda\theta_0) >+ \dot{\beta}_{1c} < -\nu \frac{\bar{\ell}^4}{4} \zeta_0 + \nu \frac{\bar{\ell}^4}{4} (\beta_0+\beta_p)\theta_0 + 2 \frac{\bar{\ell}^3}{3} + 2 \frac{\bar{\ell}^2}{2} \bar{e} + 2 \frac{1}{2} \nu \bar{b} \frac{\bar{\ell}^3}{3} \cos\theta_0 - \bar{h}_2(\bar{\ell}^2\beta_0 - \nu \frac{\bar{\ell}^3}{3} \theta_0 - \nu \frac{\bar{\ell}^2}{2} (-2\lambda+\bar{e}\theta_0))>$$

$$+ \dot{\beta}_{1s} < -2 \frac{\bar{\ell}^3}{3} \zeta_0 - \bar{g}_{SF} - \nu \frac{\bar{\ell}^4}{4} - 2\nu \frac{\bar{\ell}^3}{3} \bar{e} - \bar{h}_2 (\nu \frac{\bar{\ell}^3}{3} (\beta_p+ \beta_0) + 2 \frac{1}{2} \nu\bar{b} \frac{\bar{\ell}^2}{2} \sin\theta_0) > + \dot{\zeta}_{1c} < \nu \frac{\bar{\ell}^4}{4} \zeta_0 2\theta_0 + \beta_p\bar{g}_{SL} - \bar{h}_2(\bar{\ell}^2\zeta_0 - 2 \nu \frac{c_{d0}}{a} \frac{\bar{\ell}^3}{3} - \nu \frac{\bar{\ell}^2}{2} \lambda\theta_0) > + \dot{\zeta}_{1s} < 2 \nu \frac{\bar{\ell}^4}{4} \theta_0 - \nu \frac{\bar{\ell}^3}{3} \lambda + 2\nu \frac{\bar{\ell}^3}{3} \bar{e}\theta_0 + \bar{h}_2 \nu\beta_p \frac{\bar{\ell}^3}{3} 2\, \theta_0 >$$

$$+ \ddot{\beta}_{1c} < - \frac{\bar{\ell}^3}{3} \zeta_0 - \bar{h}_2 \frac{1}{2} \nu\bar{b} \frac{\bar{\ell}^2}{2} \sin\theta_0 >$$

$$+ \ddot{\beta}_{1s} < -\frac{\bar{\ell}^3}{3} - \frac{1}{2}\nu\bar{b}\frac{\bar{\ell}^3}{3}\cos\theta_0 - \frac{\bar{\ell}^2}{2}\bar{e}$$
$$- \bar{h}_2\beta_p\frac{\bar{\ell}^2}{2} >$$
$$+ \ddot{\zeta}_{1c} < \frac{\bar{\ell}^3}{3}(\beta_p + \beta_0) + \bar{h}_2\frac{\bar{\ell}^2}{2} >$$
$$+ \ddot{\phi} < -\frac{\bar{\ell}^3}{3} - \frac{\bar{\ell}^2}{2}\bar{e} - \bar{h}_2\beta_p\frac{\bar{\ell}^2}{2} - \bar{h}_2\frac{\bar{\ell}^2}{2}(\beta_p + \beta_0)$$
$$- \bar{h}_2\left(\frac{\bar{\ell}^2}{2}(\beta_p + \beta_0) + 2\bar{h}_2\bar{\ell}\right) >$$
$$+ \dot{\phi} < -\frac{\bar{\ell}^3}{3}2\zeta_0 - \nu\frac{\bar{\ell}^3}{3}\bar{e} - \nu\frac{\bar{\ell}^4}{4} - \bar{h}_2\beta_p\nu\frac{\bar{\ell}^3}{3}$$
$$- \bar{h}_2\beta_0\nu\frac{\bar{\ell}^3}{3} > + \ddot{\theta} < \frac{\bar{\ell}^3}{3}\zeta_0 >$$
$$+ \dot{\theta} < \nu\frac{\bar{\ell}^4}{4}\zeta_0 - 2\frac{\bar{\ell}^3}{3} - \frac{\bar{\ell}^2}{2}2\bar{e} - 2\bar{h}_2\beta_p\frac{\bar{\ell}^2}{2}$$
$$- \bar{h}_2\nu\frac{\bar{\ell}^3}{3}\theta_0 + \nu\frac{\bar{\ell}^2}{2}\lambda 2\bar{h}_2 + \bar{h}_2\nu\frac{\bar{\ell}^2}{2}\lambda$$
$$- \bar{h}_2\nu\frac{\bar{\ell}^3}{3}2\theta_0 > \}$$
$$- I_{xx}\Omega^2\ddot{\phi} + I_{xy}\Omega^2\ddot{\theta} = 0 \qquad (A.7)$$

Pitch

$$\frac{N}{2}m\Omega^2R^3\{\beta_{1c} < 2\nu\frac{\bar{\ell}^4}{4}\zeta_0 - \nu\frac{\bar{\ell}^4}{4}(\beta_p + 3\beta_0)\theta_0$$
$$- \frac{1}{2}\nu\bar{b}\frac{\bar{\ell}^3}{3}\cos\theta_0$$
$$- \bar{h}_2\left(\nu\frac{\bar{\ell}^3}{3}2\theta_0 - \frac{\bar{\ell}^2}{2}\beta_p - \bar{\ell}^2\beta_0\right.$$
$$\left. + \nu\frac{\bar{\ell}^2}{2}(-3\lambda + \bar{e}\theta_0)\right) >$$
$$+ \beta_{1s} < \nu\frac{c_{d0}}{a}\frac{\bar{\ell}^4}{4} + \nu\frac{\bar{\ell}^3}{3}\lambda\theta_0 + \bar{g}_{SF} + \nu\frac{\bar{\ell}^4}{4}$$
$$+ 2\nu\frac{\bar{\ell}^3}{3}\bar{e} + \bar{h}_2\left(\beta_p\nu\frac{\bar{\ell}^3}{3} + \beta_0\nu\frac{\bar{\ell}^3}{3}\right.$$
$$\left. + \nu\frac{\bar{\ell}^3}{3}\zeta_0\theta_0 + \frac{1}{2}\nu\bar{b}\frac{\bar{\ell}^2}{2}\sin\theta_0\right) >$$
$$+ \zeta_{1c} < -\nu\frac{\bar{\ell}^4}{4}\zeta_0 2\theta_0 - \beta_p\bar{g}_{SL} + \nu\frac{\bar{\ell}^4}{4}(\beta_p + \beta_0)$$
$$+ \bar{h}_2\left(\bar{\ell}^2\zeta_0 - 2\nu\frac{c_{d0}}{a}\frac{\bar{\ell}^3}{3} - \nu\frac{\bar{\ell}^2}{2}\lambda\theta_0\right) >$$
$$+ \zeta_{1s} < -\nu\frac{\bar{\ell}^4}{4}\theta_0 + \bar{h}_2\nu\frac{\bar{\ell}^3}{3}(-\beta_p + \beta_0)\theta_0 >$$
$$+ \dot{\beta}_{1c} < 2\frac{\bar{\ell}^3}{3}\zeta_0 + \bar{g}_{SF} + \nu\frac{\bar{\ell}^4}{4} + 2\nu\frac{\bar{\ell}^3}{3}\bar{e}$$
$$+ \bar{h}_2\left(\nu\frac{\bar{\ell}^3}{3}(\beta_p + \beta_0) + 2\frac{1}{2}\nu\bar{b}\frac{\bar{\ell}^2}{2}\sin\theta_0\right)$$
$$+ \dot{\beta}_{1s} < -\nu\frac{\bar{\ell}^4}{4}\zeta_0 + \nu\frac{\bar{\ell}^4}{4}\theta_0(\beta_p + \beta_0) + 2\frac{\bar{\ell}^3}{3}$$
$$+ 2\frac{\bar{\ell}^2}{2}\bar{e} + 2\frac{1}{2}\nu\bar{b}\frac{\bar{\ell}^3}{3}\cos\theta_0$$
$$- \bar{h}_2\left(\bar{\ell}^2\beta_0 - \nu\frac{\bar{\ell}^3}{3}\theta_0 - \nu\frac{\bar{\ell}^2}{2}(-2\lambda + \bar{e}\theta_0)\right) >$$
$$+ \dot{\zeta}_{1c} < -2\nu\frac{\bar{\ell}^4}{4}\theta_0 + \nu\frac{\bar{\ell}^3}{3}\lambda - \nu\frac{\bar{\ell}^3}{3}\bar{e}\,2\theta_0$$
$$- \bar{h}_2\beta_p\nu\frac{\bar{\ell}^3}{3}2\theta_0 >$$
$$+ \dot{\zeta}_{1s} < \nu\frac{\bar{\ell}^4}{4}\zeta_0\,2\theta_0 + \beta_p\bar{g}_{SL} - \bar{h}_2\bar{\ell}^2\zeta_0$$
$$+ \bar{h}_2\nu\frac{c_{d0}}{a}2\frac{\bar{\ell}^3}{3} + \bar{h}_2\nu\frac{\bar{\ell}^2}{2}\lambda\theta_0 >$$
$$+ \ddot{\beta}_{1c} < \frac{\bar{\ell}^3}{3} + \frac{1}{2}\nu\bar{b}\frac{\bar{\ell}^3}{3}\cos\theta_0 + \frac{\bar{\ell}^2}{2}\bar{e} + \bar{h}_2\beta_p\frac{\bar{\ell}^2}{2} >$$
$$+ \ddot{\beta}_{1s} < -\frac{\bar{\ell}^3}{3}\zeta_0 - \bar{h}_2\frac{1}{2}\nu\bar{b}\frac{\bar{\ell}^2}{2}\sin\theta_0 >$$
$$+ \ddot{\zeta}_{1s} < \frac{\bar{\ell}^3}{3}(\beta_0 + \beta_p) + \bar{h}_2\frac{\bar{\ell}^2}{2} >$$
$$+ \ddot{\phi} < -\frac{\bar{\ell}^3}{3}\zeta_0 >$$
$$+ \dot{\phi} < -\nu\frac{\bar{\ell}^4}{4}\zeta_0 + 2\frac{\bar{\ell}^3}{3} + \frac{\bar{\ell}^2}{2}2\bar{e} + 2\bar{h}_2\beta_p\frac{\bar{\ell}^2}{2}$$
$$+ \bar{h}_2\nu\frac{\bar{\ell}^3}{3}\theta_0 - \nu\frac{\bar{\ell}^2}{2}2\lambda\bar{h}_2 + \bar{h}_2\nu\frac{\bar{\ell}^3}{3}2\theta_0$$
$$- \bar{h}_2\nu\frac{\bar{\ell}^2}{2}\lambda >$$
$$+ \ddot{\theta} < -\frac{\bar{\ell}^3}{3} - \frac{\bar{\ell}^2}{2}\bar{e} - \bar{h}_2\frac{\bar{\ell}^2}{2}(\beta_p + \beta_0)$$
$$- \bar{h}_2\beta_p\frac{\bar{\ell}^2}{2} + \bar{h}_2\left(-\frac{\bar{\ell}^2}{2}(\beta_p + \beta_0) - 2\bar{\ell}\,\bar{h}_2\right) >$$
$$+ \dot{\theta} < -\frac{\bar{\ell}^3}{3}2\zeta_0 - \nu\frac{\bar{\ell}^4}{4} - \nu\frac{\bar{\ell}^3}{3}\bar{e} - \nu\frac{\bar{\ell}^3}{3}\beta_p\bar{h}_2$$
$$\left. - \nu\frac{\bar{\ell}^3}{3}\beta_0\bar{h}_2 > \right\} - I_{yy}\Omega^2\ddot{\theta} + I_{yx}\Omega^2\ddot{\phi} = 0$$
$$(A.8)$$

Appendix B: Rotor, Blade and Body Properties

Rotor Geometry

Number of blades	3
Radius, cm	81.1
Chord, cm	4.19
Hinge offset, cm	8.51
Blade airfoil	NACA 23012
Profile drag coefficient	0.0079
Lock number	7.73
Solidity ratio	0.0494
Lift curve slope	2π
Height of rotor hub above gimbal, cm	24.1

Blade Mass Properties

Blade mass (to flap flexure), gm	209
Blade mass centroid (Ref. flexure centerline), cm	18.6
Blade flap inertia (Ref. flexure centerline), gm m^2	17.3

Blade Frequency and Damping

	Conf. 1	Conf.4
Nonrotating flap freq. Hz	3.13	6.63
Nonrotating lead-lag freq. Hz	6.70	6.73
Damping in lead-lag (% critical)	0.52%	0.53%

Body Mass Properties

Rotary inertia in pitch, gm m^2	633
Rotary inertia in roll, gm m^2	183

Body Frequency and Damping

Pitch frequency, Hz	2
Roll frequency, Hz	4
Damping in roll (% critical)	0.929%
Damping in pitch (% critical)	3.20%

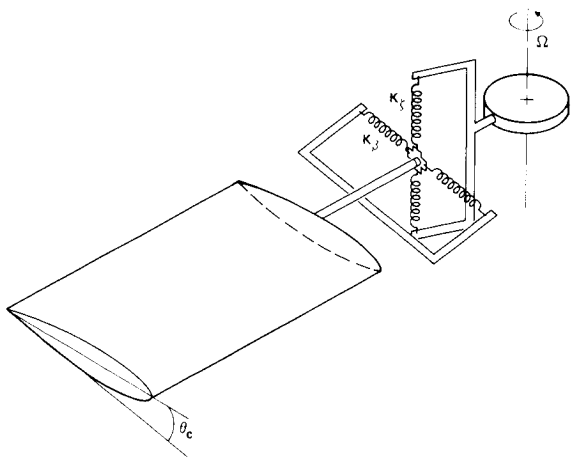

Figure 1. Equivalent Spring Restrained Blade Model.

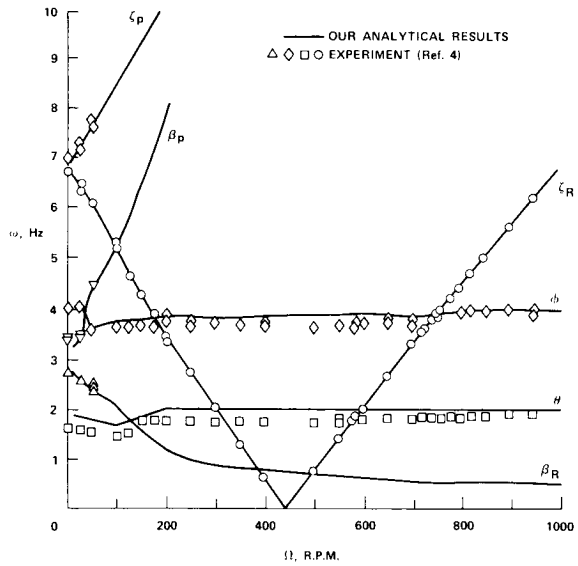

Figure 2. Modal Frequencies as a Function of Ω, θ_c = 0 (Configuration 1).

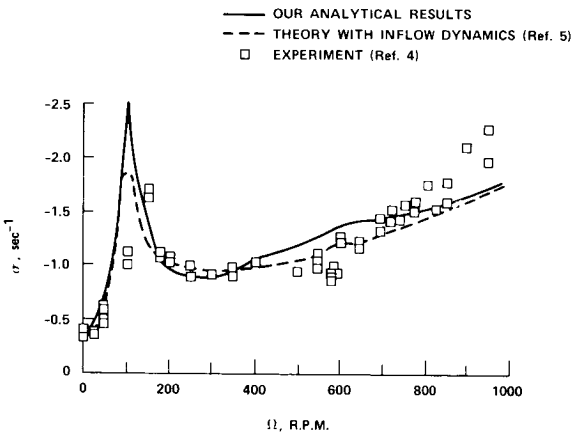

Figure 3. Body Pitch Mode Damping as a Function of Ω, θ_c = 0 (Configuration 1).

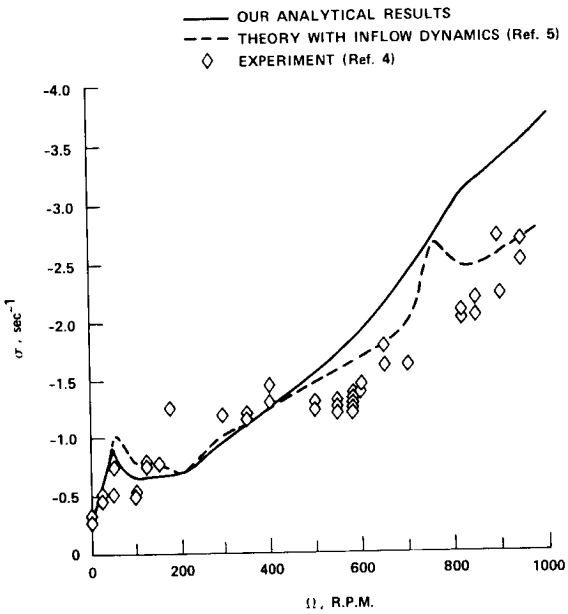

Figure 4. Body Roll Mode Damping as a Function of Ω, $\theta_c = 0$ (Configuration 1).

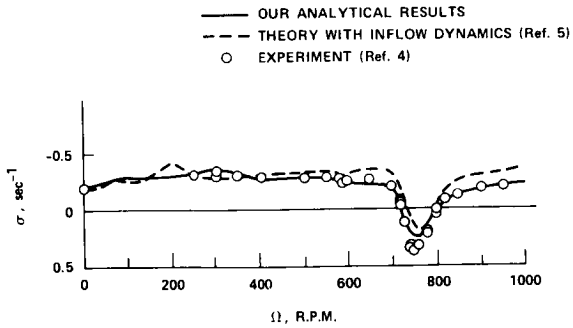

Figure 5. Regressing Lag Mode Damping as a Function of Ω, $\theta_c = 0$ (Configuration 1).

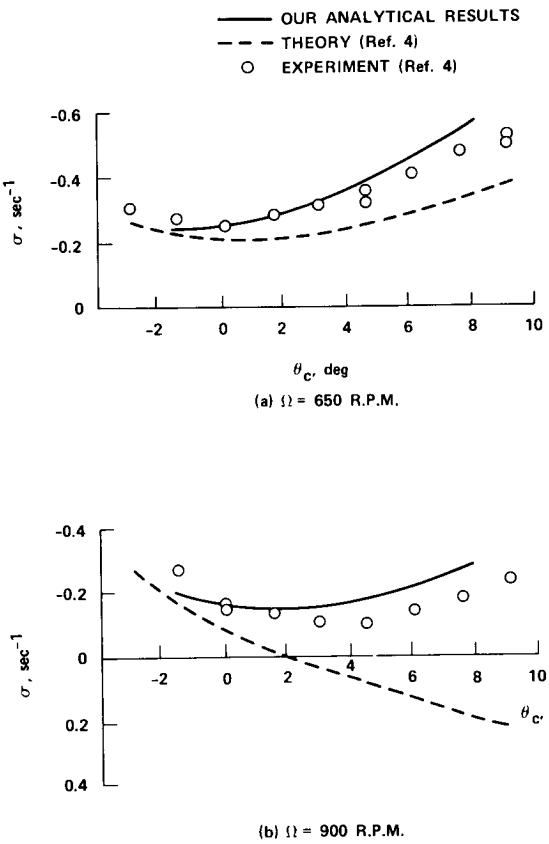

Figure 6. Lead Lag Regressing Mode Damping as a Function of θ_c at (a) 650 R.P.M. and (b) 900 R.P.M. (Configuration 1).

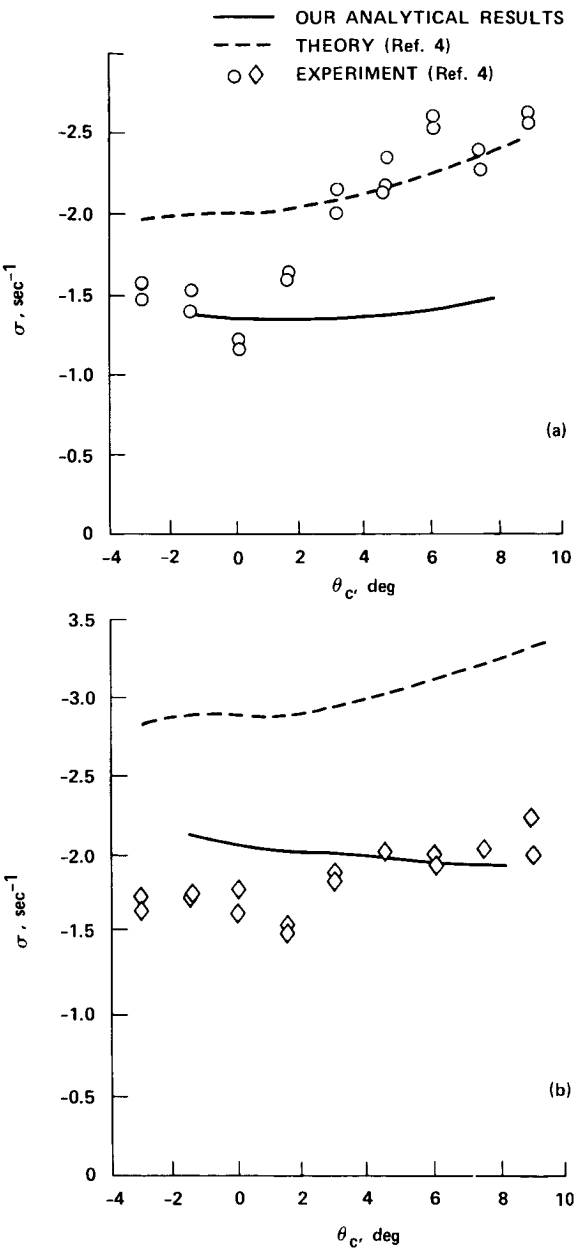

Figure 7. Variation of Damping in (a) Pitch and (b) Roll with θ_c at Ω = 650 R.P.M. (Configuration 1).

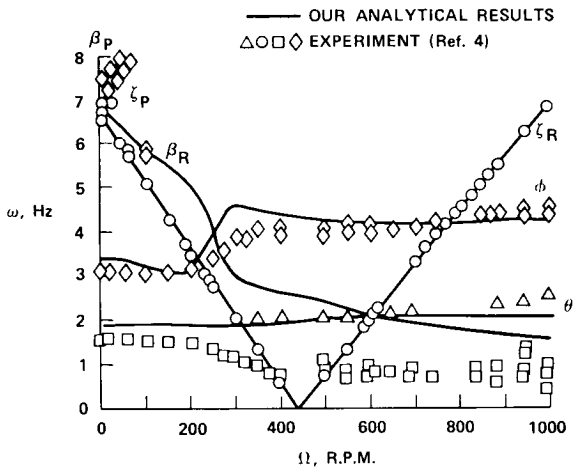

Figure 8. Variation of Modal Frequencies with Ω, θ_c = 0 (Configuration 4).

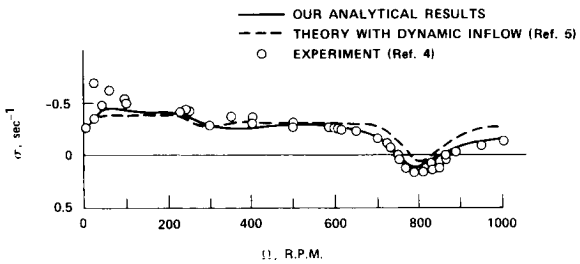

Figure 9. Variation of Damping in Lag Regressing Mode with Ω, θ_c = 0 (Configuration 4).

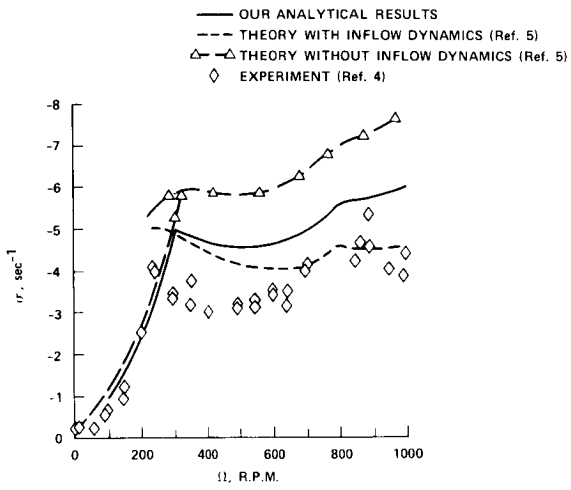

Figure 10. Variation of Damping in Roll with Ω, $\theta_c = 0$ (Configuration 4).

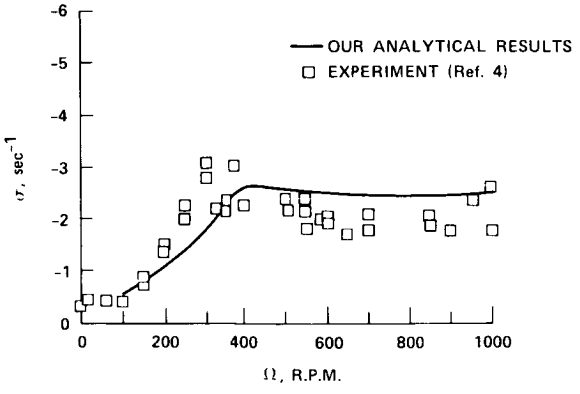

Figure 11. Variation of Damping in Pitch with Ω, $\theta_c = 0$ (Configuration 4).

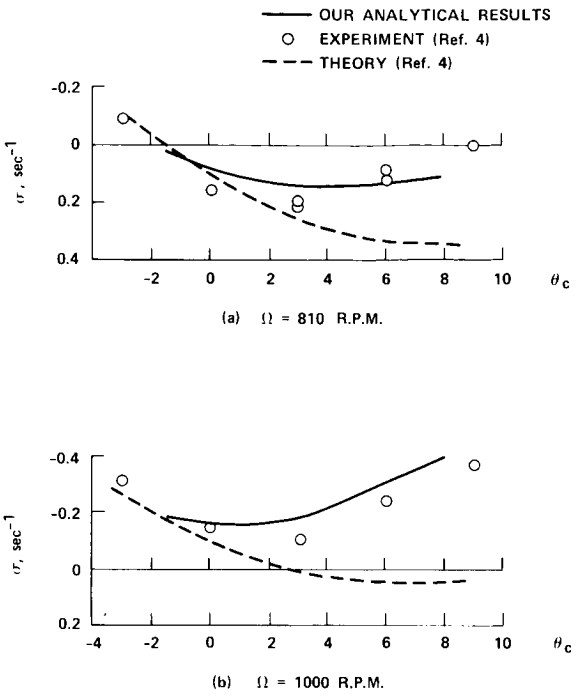

Figure 12. Variation of Damping in Lag Regressing Mode with θ_c at (a) 810 R.P.M. and (b) 1000 R.P.M. (Configuration 4).

ORIGINAL PAGE IS
OF POOR QUALITY